INTERNATIONAL JOURNAL OF HYDROGEN ENERGY 47 (2022) 4294–4303

Available online at www.sciencedirect.com

ScienceDirect

journal homepage: www.elsevier.com/locate/he

Challenges and important considerations when benchmarking single-cell alkaline electrolyzers

Cinar Karacan [a], *Felix P. Lohmann-Richters* [a], *Gareth P. Keeley* [b,1], *Fabian Scheepers* [a], *Meital Shviro* [a], *Martin Müller* [a], *Marcelo Carmo* [a,c,*,2], *Detlef Stolten* [d,e]

[a] *Forschungszentrum Jülich GmbH, Institute of Energy and Climate Research, IEK-14: Electrochemical Process Engineering, 52425 Jülich, Germany*

[b] *Univ. Grenoble Alpes, CEA, LETI, DTBS, L2CB, 38000 Grenoble, France*

[c] *Mechanical and Materials Engineering, Queen's University, Kingston, ON, K7L 3N6, Canada*

[d] *Forschungszentrum Jülich GmbH, Institute of Energy and Climate Research, IEK-3: Techno-economic Systems Analysis, 52425 Jülich, Germany*

[e] *Chair for Fuel Cells, RWTH Aachen University, Germany*

HIGHLIGHTS

- Identifying difficulties associated with the benchmarking of alkaline single cells.
- Negative effects on reproducibility observed due to reduction in conditioning time.
- A stable passivation layer of NiO on anode during long-term operation.
- Most overvoltage comes from the anode and cathode activation overpotential.
- Morphologies of substrate material exhibited an key influence on the performance.

ARTICLE INFO

Article history:
Received 1 September 2021
Received in revised form
8 November 2021
Accepted 9 November 2021
Available online 7 December 2021

Keywords:
Hydrogen
Alkaline electrolyzers
Benchmarking
Harmonization
Electrodes

ABSTRACT

This study outlines an approach to identifying the difficulties associated with the benchmarking of alkaline single cells under real electrolyzer conditions. A challenging task in the testing and comparison of different catalysts is obtaining reliable and meaningful benchmarks for these conditions. Negative effects on reproducibility were observed due to the reduction in conditioning time. On the anode side, a stable passivation layer of NiO can be formed by annealing of the Ni foams, which is even stable during long-term operation. Electrical contact resistance and impedance measurements showed that most of the contact resistance derived from the annealed Ni foam. Additionally, analysis of various overvoltages indicated that most of the total overvoltage comes from the anode and cathode activation overpotential. Different morphologies of the substrate material exhibited an influence on the performance of the alkaline single cell, based on an increase in the ohmic resistance.

* *Corresponding author*. Forschungszentrum Jülich GmbH, Institute of Energy and Climate Research, IEK-14: Electrochemical Process Engineering, 52425 Jülich, Germany.
E-mail address: m.carmo@fz-juelich.de (M. Carmo).
[1] Present Affiliation: Univ. Grenoble Alpes, CEA, LETI, DTBS, L2CB, 38000 Grenoble, France.
[2] Present Affiliation: NEL Hydrogen, Wallingford, Connecticut 06492, USA; email: mcarmo@nelhydrogen.com

https://doi.org/10.1016/j.ijhydene.2021.11.068

Introduction

Hydrogen is considered a fuel and chemical feedstock with high propositional value; an energy carrier with a high energy density and an almost infinite storage capacity [1,2]. It will enable a society based on sustainable forms of energy conversion and storage. Strong emphasis is nowadays placed on the search for the best technical solutions to cost-effectively produce "green hydrogen" using water electrolyzers. Low-temperature alkaline electrolysis is a well-established technology and has been widely used since the beginning of the last century for the electrolytic production of hydrogen at scale [3,4]. It has significant economical appeal due to the high abundance and low cost of the electrode materials used and other components based on nickel and iron, which substantially decrease the fabrication costs of large-scale electrodes. As previously noted by Smolinka et al. alkaline cells have reached electrode areas as high as 4 m^2 per cell in commercial stacks [5,6]. One disadvantage of alkaline water electrolyzers is the low performance profiles caused by the commonly-used thick diaphragms that increase ohmic resistance, the lower intrinsic conductivity of OH^- compared to H^+, and the higher gas crossover observed for highly porous diaphragms [7,8]. Due to its low current cost of 12 €·kg_{Ni}^{-1} [9] and high chemical resistance in alkaline media, nickel is the most commonly-used catalyst material. However, due to the lower intrinsic electrocatalytic activity of nickel compared to noble metals such as platinum (approximately two orders of magnitude) [9], it is often necessary to combine it with other metals to form alloys such as molybdenum, iron, aluminum, or tin [10–17]. Another common approach is to increase the surface area of the catalyst that remains exposed to the electrochemical reactants. This can be accomplished by different strategies, such as supporting the active catalyst on a carbon support [18,19], nano-engineering the catalyst morphology and structure [20–22], using novel synthesis methods to support the catalyst on 3D substrates such as nickel foam [23–26], or by exploring different catalyst deposition methods [27–31]. Therefore, a great deal of research in the field of alkaline water electrolysis has been devoted to the search for new electrocatalyst materials that are not only highly active with respect to water-splitting but also stable over the long time periods (e.g., 95.000 h) [32,33] A commonly-used way to test electrocatalysts is to utilize the so-called three-electrode setup with catalysts supported on a rotating disc electrode (RDE). A vast number of articles have reported on electrocatalysts that were investigated using such a method at relatively low electrolyte concentrations (e.g., 1 mol l^{-1}) and at room temperature, to obtain a first and rapid insight into their performance [14,15,17,20,21,24,34–36]. Unfortunately, only a few studies have attempted to properly modulate electrocatalyst performance using single cells and, more importantly, under real alkaline electrolyzer conditions [31,37–41]. In commercial electrolyzer stacks, many other parameters, such as higher gas cross-over [42], uncontrolled cell-torque conditions [43], and the interface resistances [2] can, apart from reaction kinetics, exert a critical influence on catalyst performance and durability. Hence, an electrocatalyst shown to feature superior activity in a half-cell test is by no means guaranteed to reproduce it in a full cell or electrolyzer [44]. Bender et al. [45] showed that among various published studies, a voltage difference of up to 600 mV at 1 A cm^{-2} exists, which is fully detrimental for the sake of performance comparisons among different publications. PEM water electrolysis is known for its well-stablished state-of-the-art materials; and yet, there are major deviations among the different studies. For alkaline water electrolysis, a reliable list of benchmark materials has not yet been established, and a greater need for the harmonization exists.

Herein, we report an initial approach to identifying and resolving some of the challenges inherent to the benchmarking of alkaline single cells under relevant industrial electrolyzer conditions. Such information will be of great benefit to those involved in the development of new electrocatalyst materials and other cells/stack components and will enable researchers to reliably evaluate and compare catalysts and serve as a guide to adequately increase the performance levels of low-temperature alkaline electrolysis test-rigs. Various cell-conditioning methods have been evaluated and discussed. We also investigated the passivation behavior of nickel foam for long-term operation and outline the interfacial resistances of the different cell components. The voltage loss contributions during electrolysis and the contact pressure distribution of the cell components were also analyzed. Finally, a useful comparison between this study and several single cells, stacks, and electrolyzers described in the literature and industry is performed and discussed. This work should also serve as an inspiration to other areas of research and development, not only in terms of electrochemistry but also for devices that utilize catalysts. By this, we hope to inspire harmonization-focused activities and work to establish performance and durability levels that are reliable and trustworthy, thus contributing to faster advances in technology and understanding.

Experimental

Definition of a benchmark

An in-house-designed alkaline single cell was used and is illustrated in Fig. 1. Nickel monopolar plates (MPPs) with a meandering flow-field and an area of 5 cm^2 were used. Commercial nickel foam with a thickness of 300 μm and a density of 500 g m^{-2} (Recemat BV) on the cathode side was used. A commercial Zirfon® (AGFA Perl UTP 500) was used as the diaphragm. On the anode side, the same nickel foam was used, but had previously been annealed for 24 h at 600 °C in a furnace under air conditions to completely oxidize its surface. Subsequently, the oxidized foam was welded to the anode flow-field and used in all the tests. This was performed to reduce the risk of influence being exerted by changes occurring on the anode side, so that the investigation could focus on the HER occurring on the cathode one. As gaskets, PTFE foils were used. The thickness of the PTFE foil around the nickel foams was 250 μm and, around the Zirfon®, featured a thickness of 450 μm.

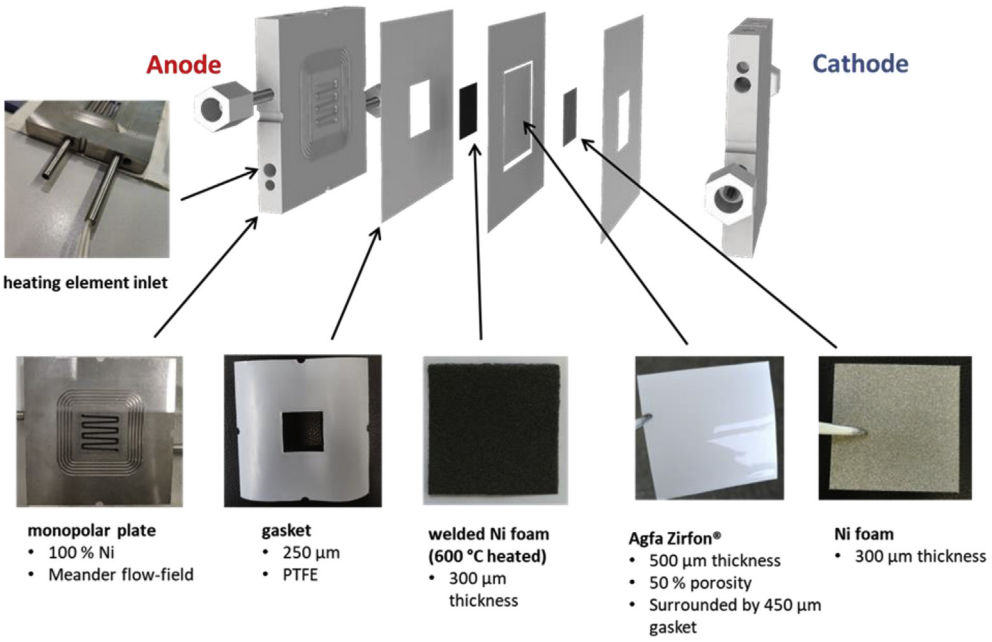

Fig. 1 – Sketch of the cell design employed in this work, along with photographs of the various components.

Electrochemical characterization

The first step was to obtain an initial performance evaluation of the benchmark using 32 cell assemblies that were individually measured using a custom-build alkaline test station. More information about the design of our in-house-developed test rigs for the benchmarking of alkaline single cells can be found in the supplementary material and information section. For each cell assembly, freshly cleaned nickel foam was used on the cathode side. Firstly, nickel foams were immersed in ethanol at ambient temperature in an ultrasonic bath for 15 min, in distilled water. Ni-foam was assembled and, after pre-heating the electrolyte to 80 °C, and a constant cell voltage of 1.7 V (Biologics BCS 815) to condition the cell was applied until the current density variation was less than 1%·hour^{-1}. The current density was changed every 5 min, and the range of 1–600 mA cm^{-2} was employed. Potentiostatic electrochemical impedance spectroscopy (IM 6 Zahner) was also performed after the cell conditioning to determine ohmic losses, which were established by fitting the Nyquist plots with a two constant phase elements model [46].

Physical characterization

The surface morphology and cross-section were examined with a scanning electron microscope (Zeiss Gemini). The through-plane resistances were measured using a typical four-point electrode setup [47]. The through-plane resistance was measured for contact pressures of between 1 and 4.5 MPa. To determine the interface resistance between the anode MPP and annealed nickel foam, the annealed nickel foam was sandwiched between two used anode MPPs. The contact resistance was measured with the same setup as previously described. The same experiment was also used for a fresh nickel foam sandwiched between two cathode MPPs to determine the interface resistance between the cathode MPP and nickel foam.

Results and discussion

Conditioning of single cells

Fig. 2a displays the cell conditioning curve aimed at a current density variation of less than 1% per hour, which was only achieved after a conditioning period of 28 h. Fig. 2b depicts the cell conditioning curve after 5 h, and Fig. 2c for the first 2 min. All three procedures were potentiostatic at a cell voltage of 1.7 V. Cell conditioning is a crucial step in cell performance evaluation. A dramatic drop in performance occurs within the first few hours. It is paramount that a stable cell condition is established prior to performance testing being performed. In this work, a current density variation of less than 1% per hour was chosen as the target for cell conditioning [45]. This threshold was chosen because it entails time-independent conditioning and electrodes with different conditioning responses can be treated electrochemically in the same manner. To reach the threshold of 1% change, the single cells had to run for up to 28 h at a 1.7 V cell voltage, as is illustrated in Fig. 2a. To observe the influence of a shorter cell conditioning time, a second cell was conditioned for 5 h at 1.7 V, as is shown in Fig. 2b. The inset of Fig. 2a shows the cell conditioning curve for the last 4 h and the change in the current density per hour, which also represents the deactivation rate of the single cell. It is apparent from Fig. 2 that the deactivation rate decreased after 28 h, (down from 213 to 11 µA cm^{-2} h^{-1}), and 20 times higher compared to the deactivation rate of a current density variation of less than 1% per hour. These findings demonstrate how important proper cell conditioning is, and a high deactivation rate is still present after 5 h of cell conditioning.

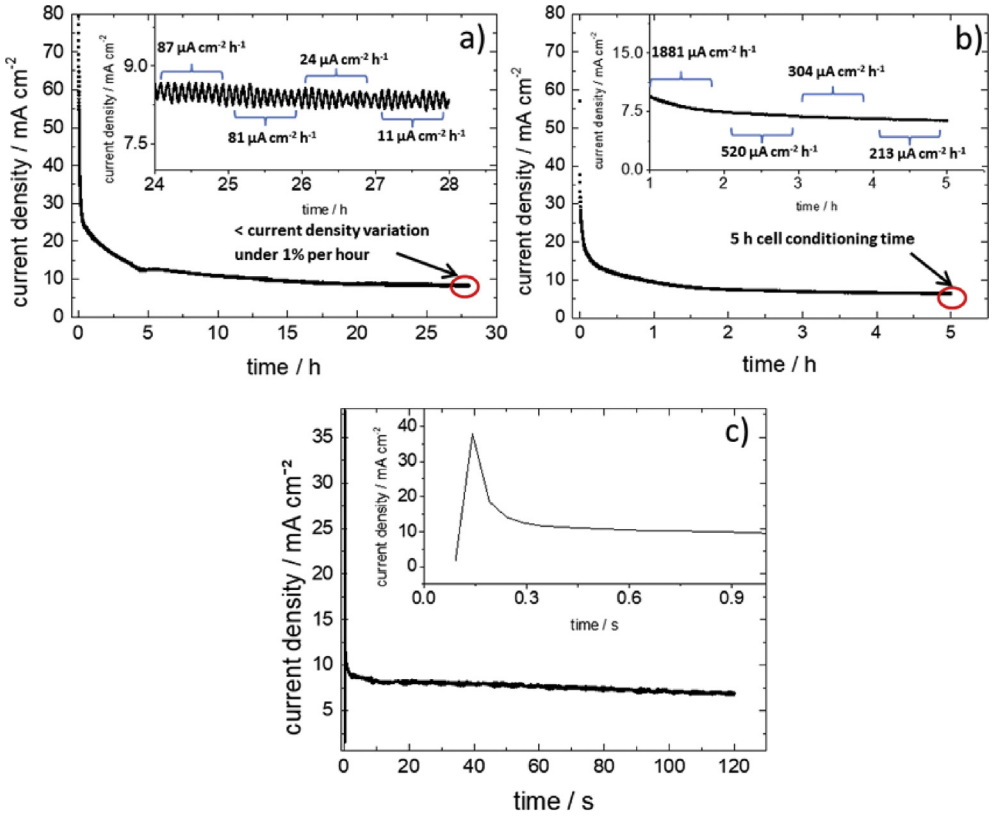

Fig. 2 – a) Example of a cell conditioning curve with a current variation under 1% per hour at a cell voltage of 1.7 V. The inset represents a zoom-in on the last four conditioning hours with deactivation rates for each hour. b) Example of a cell conditioning curve with a 5 h conditioning time at a cell voltage of 1.7 V. The inset represents a zoom-in on the last four conditioning hours with deactivation rates for each. c) Example of a cell conditioning curve at a voltage of 1.7 V for the first 2 min. The inset represents a zoom-in on the first second of the cell conditioning curve.

Therefore, running a polarization curve based on a short conditioning time may not represent an accurate figure of merit with respect to cell performance.

Nevertheless, the largest current drop occurred at the beginning of the cell conditioning. Therefore, a shorter cell conditioning was considered to allow for comparisons with previous studies. Fig. 2c depicts the cell conditioning for the first 2 min. The inset diagram in the Fig. 2 shows the extent to which cell deactivation occurs within the first few seconds. Several mechanisms influence the conditioning curve or deactivate and degrade the electrodes:

(1) Bubble coverage by product gases.
(2) Absorption of atomic hydrogen in the nickel lattice (cathode).
(3) Changes in the Ni^{2+} oxide layer (anode).
(4) Loss of active catalyst material due to mechanical or chemical stresses.

After the formation of the double layer, a sharp current drop is observed, which decreases exponentially with time. (1) One reason for the sharp initial current drop is bubble coverage of the active layer [48–50]. Vogt et al. showed that a nickel plate operating as a cathode for 1 h and then being switched to an anode electrode took 45 min to reach steady-state bubble coverage in a stagnant electrolyte [49]. Zhang et al. showed that a bubble "curtain" exists on the electrode, even at higher current densities and when the electrolyte is flowing, which can be attributed to the continuous formation of new bubbles [51]. Unfortunately, these studies were only performed on electrodes that featured an inter-electrode gap. The product gas bubbles could be trapped between the pores in highly porous 3D structures, such as the nickel foam used in this work. Trapped gas bubbles cannot be removed by means of simple electrolyte flow or gas buoyancy in liquid media, as it becomes part of complex two-phase flow phenomena attached to gas absorption behaviors and may be a more serious problem than in the case with nonporous layers, such as the perforated electrodes typically used in commercial stacks. Phillips et al. showed that nickel foams exhibit higher ohmic resistance at higher current densities than other nickel substrates, such as expanded metals or woven structures, and that the foam is clogged by trapped gas bubbles and the active surface area decreases with increasing gas evolution [52]. Therefore, it is vital to study and understand the mechanisms of the bubble coverage within foam structure, as nickel foam is regularly used as a catalyst-coated substrate electrolyzers at lab-scale [22,53–57]. The bubble coverage is assumed to reach a stationary state and appears to play a minor role in the deactivation rate. Hence, mechanisms (2), (3), and (4) act as soon as electrolysis starts, gradually deactivating the electrodes.

(2) is the absorption of atomic hydrogen in the nickel lattice [58–60]. The formation of β-nickel hydride is known to act as a diffusion barrier against further hydrogen penetration and causes deactivation of the cathode catalyst [61]. Thus, mechanism (2) would be strongly represented when cell conditioning begins. Therefore, after conditioning, when the reaction rate of β-nickel hydride formation is reduced, such a mechanism would contribute to a small fraction of the degradation of the nickel foam.

(3) The surface structure of the anode electrode can be changed by it oxidizing at different potentials. Hall et al. showed that NiO and α-$Ni(OH)_2$ are formed with increasing anodic potential. Subsequently, β-$Ni(OH)_2$ can be chemically-formed from α-$Ni(OH)_2$, and NiOOH can be formed from α/β-$Ni(OH)_2$ as the electric potential increases [62], and is strongly responsible for further deactivation of the anode electrode, as the later species are much less active and possess lower surface areas.

(4) Loss of active catalyst material due to successive mechanical and/or chemical erosion of nickel particles is a major problem, especially in coated porous substrates, and is a major factor in electrode degradation at lab-scale. As the nickel foam was not coated with a catalyst for the experiments performed in this study, this degradation mechanism plays no role during the cell conditioning period.

In summary, we attribute the degradation and deactivation mechanisms (1), (2) and (3) to the sharp drop in current at the beginning of the cell conditioning.

Baseline of single cells

Figure a shows the mean polarization curve from 32 cell assemblies after reaching a current variation of less than 1% per hour (28 h) and the curve with the average for a cell conditioning procedure of 5 h, resulting 2.00 ± 0.020 V at 300 mA cm^{-2}. Baseline reproducibility is an essential aspect related to the minimization of the potential influence of the overall test rig system and cell assembly on the performance deviation from one cell to another. This ensures that the observed performance deviation while evaluating other electrodes can be explicitly attributed to variations in the electrocatalyst material employed. Failure to do this would expose the results to the vagaries of, for instance, unstable temperature control, electrolyte concentration changes during measurements, and material deviation of the components used in the cell or cell tightness. For a 5 h cell conditioning time, the current density variation was found to be 2–5% per hour. The cell voltage was 1.99 ± 0.025 V at 300 mA cm^{-2}. Shortening the cell conditioning time to 5 h significantly changed the reproducibility. It has not yet been clarified which mechanism has an impact on reproducibility but based on the literature, a few assumptions can be made. Rommal et al. showed, in a galvanostatically-controlled setup, that the absorption rate of hydrogen into a nickel foil decreases over time. This was explained by the formation of β-nickel hydride, which is used as a diffusion barrier against further hydrogen penetration [61]. As described in the conditioning procedure, bubble coverage (1) can take 45 min to reach a steady state in a stagnant electrolyte [48]. Based on this study, bubble coverage would only affect reproducibility when the conditioning time is short. However, it is worth noting that the bubble coverage behavior can differ when a non-stagnant electrolyte and zero-gap assembly are used. This shows that a sensible conditioning time for single cells is crucial to avoiding misleading performance curves. A shorter conditioning time would lead to unacceptable reproducibility, which can be a particular problem for new electrodes with unknown properties, which often suffer from poor reproducibility. Finally, it is difficult to determine whether the lack of reproducibility is due to the electrode fabrication, the used test protocol, or the cell/system setup.

Impact of electrolyte flow rates on the benchmark

At this stage, the selected protocol was modified, with the electrolyte flow varied to 2.0 and 0.2 ml $cm^{-2}\cdot min^{-1}$, from an original electrolyte flow rate of 20 ml $cm^{-2}\cdot min^{-1}$. The objective here was to determine the effect of a reduced electrolyte flow rate. The pumps of an electrolyzer belong to the unit's peripheral units and play an important role in its total cost. The operating cost increases with the flow rate. Therefore, electrolyzer designs aim to keep the electrolyte pumping rate as low as possible, while still ensuring a proper supply of water to the electrodes.

Based on the polarization curves shown in Fig. 3b, it is apparent that at lower current densities (50–200 mA cm^{-2}), the electrolyte flow rates of 0.2 and 2.0 ml $cm^{-2}\cdot min^{-1}$ improve the performance of the benchmark cell. Here, the electrolyte flow rate of 2.0 ml $cm^{-2}\cdot min^{-1}$ exhibited a reduction in cell voltage of 30 mV at a current density of 200 mA cm^{-2} compared to the highest electrolyte flow rate. As the current density increases, so does the reduction in cell voltage. Here, at a current density of 250 mA cm^{-2}, the performance of the benchmark cell with an electrolyte flow rate of 0.2 ml $cm^{-2}\cdot min^{-1}$ is as high as for an electrolyte flow rate of 20 ml $cm^{-2}\cdot min^{-1}$. At higher current densities, the performance for an electrolyte flow rate of 0.2 ml $cm^{-2}\cdot min^{-1}$ is worse than at 20 ml $cm^{-2}\cdot min^{-1}$. At a current density of 600 mA cm^{-2}, the difference in cell voltage for an electrolyte flow rate of 2 ml $cm^{-2}\cdot min^{-1}$ is only minor compared to one of 20 ml $cm^{-2}\cdot min^{-1}$, considering the statistical deviation.

Phillips et al. showed that a low flow rate greatly increases the ohmic resistance for a cell array with an electrode spacing of 2 mm [52], explained by the fact that a higher flow rate reduces the void fraction, which affects the ohmic resistance. Hence, at lower electrolyte flow rates, even for zero-gap arrays, as the current density increases, the ohmic resistance becomes higher.

Physical characterization of the benchmark

Fig. 4a–4l show SEM cross-sectional images of the nickel foam used in the benchmark under different operating conditions. The corresponding elemental analyses recorded in EDS for the oxygen and nickel elements are shown. Fig. 4a displays a cross-sectional image of the cleaned nickel foam, the thickness of whose struts is about 20–25 μm. Fig. 4b and c shows

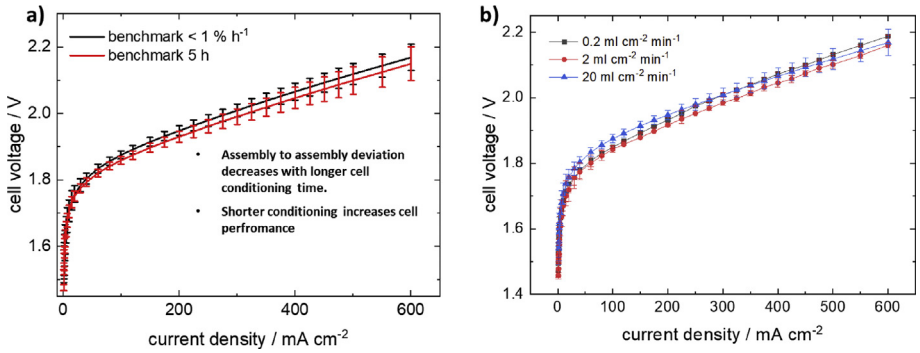

Fig. 3 – a) Polarization curve of the baseline with cell conditioning of a current variation under 1% per hour and the baseline for the cell conditioning procedure of 5 h. Error bars represent the standard deviation of at least 32 cell assemblies. b) The error bars represent the standard deviation of at least three cell assemblies.

the EDS elemental analyses where only nickel was detected. Fig. 4d–f shows the cross-section of the nickel foam preheated at 600 °C. Fig. 4e and f shows an oxide passivation layer on the surface of the nickel foam with a thickness of 1–5 μm. Atkinson et al. heated polycrystalline nickel sheets at various temperatures and holding times under an oxygen atmosphere at 1 atm and observed a linear increase in the NiO passivation layer thickness with the time and temperature. A layer thickness of 3.3 μm was reported at a temperature of 600 °C and a heating time of 29 h, which is consistent with the results reported herein [63]. Fig. 4g–i shows a cross-section of the nickel foam preheated at 600 °C after 1000 h at a 2 V cell tension. The oxide layer (1–7 μm) did not significantly change following the treatment. Fig. 4k and l shows a cross-section of a non-preheated anode nickel foam after 1000 h at a cell voltage of 2 V. The oxygen EDS elemental analysis demonstrates that the oxide layer thickness is less than 1 μm, which is much thinner than the preheated (Fig. 4h) nickel foam.

Fig. 4m–p shows the corresponding XRD diffractograms of the nickel foams. The diffractogram of the nickel foam preheated at 600 °C (Fig. 4n) exhibits strong nickel and weaker NiO reflections. This corresponds to the result of the EDS elemental analysis (Fig. 4e and f), where a NiO passivation layer was found. Preheating of the nickel foam resulted in a thickness for which no further electrochemical passivation occurred at a cell voltage of 2 V. However, higher cell voltages may lead to an increase in the NiO_x thickness. These observations would explain why the passivation layer of the preheated nickel foam did not change after 1000 h of constant cell voltage. The diffractogram of the non-preheated anode nickel

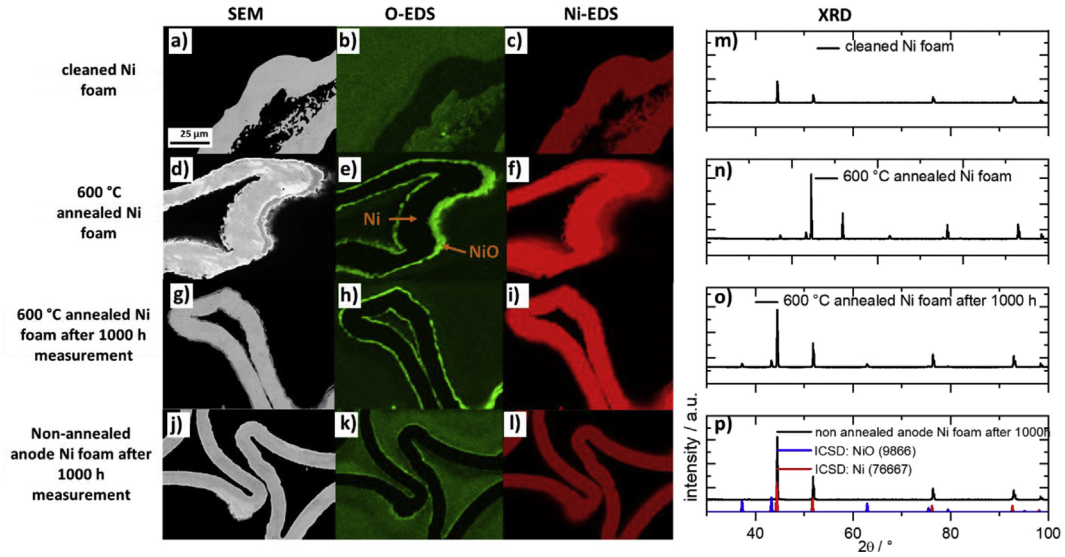

Fig. 4 – SEM cross-sections of: a) Cleaned nickel foam; b) an oxygen EDS elemental analysis of the purified nickel foam; c) a nickel EDS elemental analysis of the purified nickel foam; d) the 600 °C preheated nickel foam; e) an oxygen EDS elemental analysis of the 600 °C preheated nickel foam; (f) a nickel EDS elemental analysis of the 600 °C preheated nickel foam; (g) the 600 °C preheated nickel foam after 1000 h of long-term measurements; (h) an oxygen EDS elemental analysis of the 600 °C preheated nickel foam after 1000 h of long-term measurements; and (i) a nickel EDS elemental analysis of the 600 °C preheated nickel foam after 1000 h of long-term measurements. The scale bar in Fig. 4a applies to all images. X-ray diffractograms for: m) cleaned nickel foam; n) 600 °C preheated nickel foam; o) 600 °C preheated nickel foam after a 1000-h long-term test; and p) non-preheated anode nickel foam after 1000 h, in Ni (red) and NiO (blue) reference samples.

Table 1 – Cell voltage at 300 mA cm^{-2} for different cell assemblies.

Cell assembly [Anode | Cathode]	Cell voltage @ 300 mA cm^{-2} [V]	Slope between 200–600 mA cm^{-2} [mΩ·cm^2]
600 °C annealed nickel foam | nickel foam (500 g m^{-2})	2.00 ± 0.020	0.74
600 °C annealed nickel foam | nickel foam (1000 g m^{-2})	2.05 ± 0.023	0.70
Perforated nickel plate | perforated nickel plate	2.06 ± 0.012	0.52
600 °C annealed nickel foam | no substrate	2.02 ± 0.017	0.46
No substrate | no substrate	1.99 ± 0.008	0.56

foam after 1000 h at 2 V also exhibited no NiO reflections. As previously noted for the deactivation mechanism (3) on the anode side, the NiO_x layer increases as a function of the applied electric potential. The dependence of the passivation thickness on the applied cell voltage would also explain why the non-preheated nickel foam (Fig. 4k) has a thinner passivation layer on the anode side than the preheated nickel foam (Fig. 4e and h). This thin passivation layer would also explain why the NiO is not visible in the diffractogram (Fig. 4p), as the XRD is not a surface-sensitive characterization method.

The influence of electrode morphologies

The same measurement protocol was applied with different electrodes and cell assemblies to determine if the morphology of the nickel substrate used had a significant impact on the performance. The results are presented in Table 1.

The results indicate that the type of uncoated electrodes used here influences the cell's performance. A perforated nickel plate (300 μm thickness) was utilized as the electrode for the anode and cathode. In addition, a nickel foam with a density of 1000 g m^{-2} was used to investigate the effect of the porosity of the nickel foam on the single cell's performance. To determine whether a nickel substrate has a beneficial effect on the single cell's performance, the cathode side was assembled without a nickel substrate and the nickel flow field was used as the electrode. In another cell assembly, the anode nickel foam preheated at 600 °C was also omitted. Fig. 5a displays the polarization curves of the cell assemblies with 1000 g m^{-2} perforated nickel plate and the benchmark, and Fig. 5b shows the polarization curves of the cell assemblies without cathode nickel foam and nickel substrate compared to the benchmark cell.

The perforated nickel plates increased the cell voltage by 60 mV at a current density of 300 mA cm^{-2} compared to the benchmark cell. The slope of 0.74 mΩ cm^2 in the regression range between 200 and 600 mA cm^{-2} is 25% greater than that of the benchmark cell. This is attributed to the much smaller contact area of the incompressible Ni flow field compared to the Ni-foam and thus introduces a higher ohmic resistance.

The cell voltage of the nickel foam with 1000 g m^{-2} is 50 mV higher than the benchmark cell using a nickel foam with a density of 500 g m^{-2} at a current density of 300 mA cm^{-2}. A possible explanation for this could be that the active surface area is more reduced in a zero-gap configuration due to the compression of the nickel foam compared to a less dense nickel foam. Phillips et al. showed that the electrode morphology has a significant effect on the ohmic resistance of the cell, especially with different current density sections [52]. With a slope of 0.70 mΩ cm^2, this is 20% higher than that of the benchmark cell.

Omitting the nickel foam on the cathode indicated that the overvoltage of the single cell was increased by 20 mV at a current density of 300 mA cm^{-2}. One explanation for this could be that the bubble coverage on the nickel foam may reduce the active surface area during electrolysis to such an extent that the increased surface area has no significant effect on performance after conditioning. It should be noted that because our cell flow field is made of nickel, the flow field is also electrochemically-active. When there is a nickel

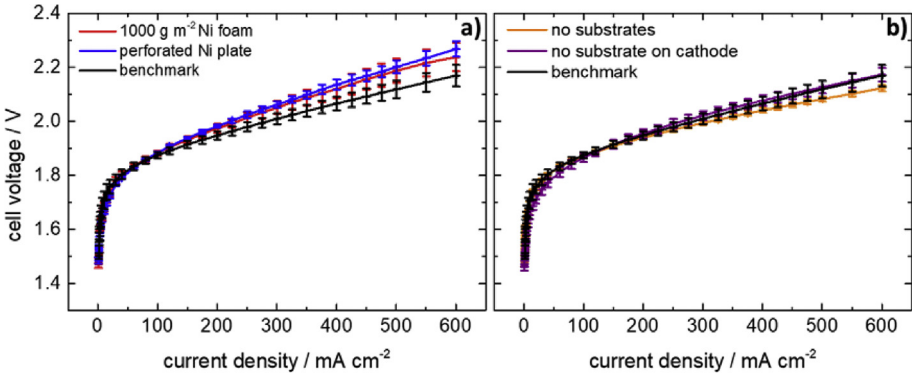

Fig. 5 – Polarization curves of cell assemblies (anode | cathode) with a) 600 °C annealed nickel foam | nickel foam (1000 g m^{-2}) (red), perforated nickel plate | perforated nickel plate (blue), and the benchmark cell (black). The inset describes a zoom-in on the low current density section. b) 600 °C annealed nickel foam | no substrate (purple), no substrate | no substrate (orange), and the benchmark cell (black). The error bars represent the standard deviation of at least three of the cell assemblies.

foam on the flow-field, it covers a significant portion of the latter's active surface area. With the added effect of the bubble coverage of the nickel foam, the total electrochemically-active surface area of the nickel foam can be reduced to the geometric surface area of the Ni flow-field. Due to the complex processes that can occur within a cell, a more detailed investigation of the bubble behavior in the zero-gap configuration with different substrate morphologies is required. However, the study of gas bubble evolution in the cavities of the nickel foam would have implications for numerous studies in which nickel foam has been used as a substrate for electrocatalysts in alkaline electrolysis cells [22,53–55,57].

If the preheated anode nickel foam is also removed, the overvoltage decreases by 10 mV compared to the benchmark cell. This is not significant though, considering the statistical imprecision. However, the polarization curve shows that the slope of 0.46 mΩ cm^{-2} is the lowest of all the cell assemblies studied. The slope of the ohmic region is significantly lower, as it contributes to a higher ohmic resistance throughout the cell due to the presence of the oxidized layer. More information and a comprehensive analysis of how the interface resistances were measured and calculated can be found in the supplementary material and information section.

Conclusions

In this study, we proposed as a first step to harmonize a single-cell test platform with the purpose to investigate electrocatalyst materials for classic alkaline electrolyzers. We found that the typically used short conditioning time has a dramatic negative impact on the reproducibility of polarization curves, which indicates that a sufficient conditioning time for single cells is crucial to avoiding misleading performance data. A conditioning method with a current density variation of less than 1% per hour was then chosen in this work for the further investigation of our electrode systems. However, the conditioning time can be made flexible, especially important for electrodes with higher degradation rates, as a too quick recording of the polarization curve would lead to incorrect conclusions with respect to cell performance. In other words, one needs to make sure the components present an acceptable level of stability before performing any performance tests.

Different morphologies of the substrate material and different cell assemblies exhibited an influence on the performance of the alkaline single cell stemming from the increase in ohmic resistance. Such effect is especially relevant for the anode side where significant material oxidation/passivation occur. SEM and XRD measurements showed that preheating the anode nickel foam can form a stable passivation layer of NiO, which is stable in the long term, even after electrochemical treatment. This guarantees a reproducible anode electrode, which is essential for the investigation of HER catalysts in a single cell. On the cathode side, we showed the importance to use of a higher density nickel foam as it decreases the possibility to have product gases trapped within the pores of the foam, thereby reducing the cell performance.

Finally, we have shown that electrocatalysts can indeed be properly evaluated for performance and durability using single-cell testing platforms. These results expand the options available to researchers for characterizing new electrocatalysts. Our simple setup for test-station, single cell architecture, and test protocols reported here can also be easily adapted to enable OER studies, not only for classical alkaline electrolysis but also with when using ion solvating membranes, AEM water electrolyzers, and other similar electrochemical devices.

Declaration of competing interest

The authors declare that they have no known competing financial interests or personal relationships that could have appeared to influence the work reported in this paper.

Acknowledgment

The authors gratefully acknowledge experimental support from Daniel Holtz, Norbert Commerscheidt, Sebastian Holtwerth, and Andreas Everwand. We would also like to convey our thanks to the HYPOS Hydrogen Power Storage & Solutions East Germany initiative, funded by the German Federal Ministry of Education and Research (BMBF) as part of the "Twenty 20 - Partnership for Innovation" program, within the framework of the ELKE Project #03ZZ0704A.

REFERENCES

[1] Schlapbach L, Züttel A. For mobile applications. Nature 2001;414(November):353–8. https://doi.org/10.1038/35104634.
[2] Ayers K, Danilovic N, Carmo M, Ryan Ouimet, Pivovar B, Bornstein M. Perspectives on low-temperature electrolysis and potential for renewable hydrogen at scale. Annu Rev Chem Biomol Eng 2019;10(1):219–39. https://doi.org/10.1146/annurev-chembioeng-060718-030241.
[3] Zhang X, Chan SH, Ho HK, Tan SC, Feng Z. Towards a smart energy network: the roles of fuel/electrolysis cells and technological perspectives. Int J Hydrogen Energy 2015;40(21):6866–919. https://doi.org/10.1016/j.ijhydene.2015.03.133.
[4] Kraglund MR, Carmo M, Schiller G, Ansar SA, Aili D, Christensen E, Jensen JO. Ion-solvating membranes as a new approach towards high rate alkaline electrolyzers. Energy Environ Sci 2019. https://doi.org/10.1039/c9ee00832b.
[5] Smolinka TFI, Günther M, Fraunhofer I, Garche J, Fcbat). Stand und entwicklungspotenzial der Wasserelektrolyse Zur Herstellung von Wasserstoff aus regenerativen energien. NOW-Studie 2011;2010:53.
[6] IRENA. Renewable Capacity Statistics. 2021. p. 2021.
[7] Guillet N, Millet P. Alkaline water electrolysis. In: Hydrogen production: electrolysis; 2015. p. 117–66.
[8] Schalenbach M, Tjarks G, Carmo M, Lueke W, Mueller M, Stolten D. Acidic or alkaline? Towards a new perspective on the efficiency of water electrolysis. J Electrochem Soc 2016;163(11):F3197–208. https://doi.org/10.1149/2.0271611jes.
[9] Quaino P, Juarez F, Santos E, Schmickler W. Volcano plots in hydrogen electrocatalysis-uses and abuses. Beilstein J

Nanotechnol 2014;5(1):846–54. https://doi.org/10.3762/bjnano.5.96.
[10] Divisek J, Mergel J, Schmitz H. Advanced water electrolysis and catalyst stability under discontiniuous operation 1990;15(2):105–14.
[11] Tanaka SI, Hlrose N, Tanaki T. Evaluation of raney-nickel cathodes prepared with aluminum powder. Denki Kagaku 1997;65(8):637–42. https://doi.org/10.5796/kogyobutsurikagaku.65.637.
[12] Tanaka S ichi, Hirose N, Tanaki T, Ogata YH. Effect of tin ingredients on electrocatalytic activity of raney-Ni prepared by mechanical alloying. Int J Hydrogen Energy 2001;26(1):47–53. https://doi.org/10.1016/S0360-3199(00)00052-5.
[13] Tanaka SI, Hirose N, Tanaki T, Ogata YH. Effect of Ni-Al precursor alloy on the catalytic activity for a raney-Ni cathode. J Electrochem Soc 2000;147(6):2242–5. https://doi.org/10.1149/1.1393514.
[14] Raj IA. Nickel-based, binary-composite electrocatalysts for the cathodes in the energy-efficient industrial production of hydrogen from alkaline-water electrolytic cells. J Mater Sci 1993;28(16):4375–82. https://doi.org/10.1007/BF01154945.
[15] Arul Raj I, Venkatesan VK. Characterization of nickel-molybdenum and nickel-molybdenum-iron alloy coatings as cathodes for alkaline water electrolysers. Int J Hydrogen Energy 1988;13(4):215–23. https://doi.org/10.1016/0360-3199(88)90088-2.
[16] Friebel D, Louie MW, Bajdich M, Sanwald KE, Cai Y, Wise AM, Cheng MJ, Sokaras D, Weng TC, Alonso-Mori R, Davis RC, Bargar JR, Nørskov JK, Nilsson A, Bell AT. Identification of highly active Fe sites in (Ni,Fe)OOH for electrocatalytic water splitting. J Am Chem Soc 2015;137(3):1305–13. https://doi.org/10.1021/ja511559d.
[17] McKone JR, Sadtler BF, Werlang CA, Lewis NS, Gray HB. Ni-Mo nanopowders for efficient electrochemical hydrogen evolution. ACS Catal 2013;3(2):166–9. https://doi.org/10.1021/cs300691m.
[18] Ahn SH, Lee BS, Choi I, Yoo SJ, Kim HJ, Cho EA, Henkensmeier D, Nam SW, Kim SK, Jang JH. Development of a membrane electrode assembly for alkaline water electrolysis by direct electrodeposition of nickel on carbon papers. Appl Catal B Environ 2014;154–155:197–205. https://doi.org/10.1016/j.apcatb.2014.02.021.
[19] Wang X, Li W, Xiong D, Petrovykh DY, Liu L. Bifunctional nickel phosphide nanocatalysts supported on carbon fiber paper for highly efficient and stable overall water splitting. Adv Funct Mater 2016;26(23):4067–77. https://doi.org/10.1002/adfm.201505509.
[20] Zhou W, Wu XJ, Cao X, Huang X, Tan C, Tian J, Liu H, Wang J, Zhang H. Ni3S2 nanorods/Ni foam composite electrode with low overpotential for electrocatalytic oxygen evolution. Energy Environ Sci 2013;6(10):2921–4. https://doi.org/10.1039/c3ee41572d.
[21] Tang C, Cheng N, Pu Z, Xing W, Sun X. NiSe nanowire film supported on nickel foam: an efficient and stable 3D bifunctional electrode for full water splitting. Angew Chem Int Ed 2015;54(32):9351–5. https://doi.org/10.1002/anie.201503407.
[22] Zhang B, Xiao C, Xie S, Liang J, Chen X, Tang Y. Iron-nickel nitride nanostructures *in situ* grown on surface-redox-etching nickel foam: efficient and ultrasustainable electrocatalysts for overall water splitting. Chem Mater 2016;28(19):6934–41. https://doi.org/10.1021/acs.chemmater.6b02610.
[23] Liu X, Wang X, Yuan X, Dong W, Huang F. Rational composition and structural design of *in situ* grown nickel-based electrocatalysts for efficient water electrolysis. J Mater Chem A 2015;4(1):167–72. https://doi.org/10.1039/c5ta07047c.
[24] Hwang B-J, Lin M-C, Lu B, Kapusta R, Wu Y, Cowley S, Dai H, Wang D-Y, Zhou W, Kenney MJ, Yang J, Gong M. Blending Cr2O3 into a NiO-Ni electrocatalyst for sustained water splitting. Angew Chem Int Ed 2015;54(41):11989–93. https://doi.org/10.1002/anie.201504815.
[25] Zhang JG, Zhang SM, Li S, Dai H, Hu Q, Zhang B, Wang LM. Electrocatalytic properties of nickel foam-based Ni-Mo, Ni+Mo and Ni+Mo/Ni-Mo electrodes for hydrogen evolution reaction. Mater Sci Forum 2018;921 MSF:134–40. https://doi.org/10.4028/www.scientific.net/MSF.921.134.
[26] You B, Jiang N, Sheng M, Bhushan MW, Sun Y. Hierarchically porous urchin-like Ni2P superstructures supported on nickel foam as efficient bifunctional electrocatalysts for overall water splitting. ACS Catal 2016;6(2):714–21. https://doi.org/10.1021/acscatal.5b02193.
[27] Bernäcker CI, Rauscher T, Büttner T, Kieback B, Röntzsch L. A powder metallurgy route to produce raney-nickel electrodes for alkaline water electrolysis. J Electrochem Soc 2019;166(6):F357–63. https://doi.org/10.1149/2.0851904jes.
[28] Siwek KI, Eugénio S, Santos DMF, Silva MT, Montemor MF. 3D nickel foams with controlled morphologies for hydrogen evolution reaction in highly alkaline media. Int J Hydrogen Energy 2019;44(3):1701–9. https://doi.org/10.1016/j.ijhydene.2018.11.070.
[29] Chade D, Berlouis L, Infield D, Cruden A, Nielsen PT, Mathiesen T. Evaluation of raney nickel electrodes prepared by atmospheric plasma spraying for alkaline water electrolysers. Int J Hydrogen Energy 2013;38(34):14380–90. https://doi.org/10.1016/j.ijhydene.2013.09.012.
[30] Kjartansdóttir CK, Nielsen LP, Møller P. Development of durable and efficient electrodes for large-scale alkaline water electrolysis. Int J Hydrogen Energy 2013;38(20):8221–31. https://doi.org/10.1016/j.ijhydene.2013.04.101.
[31] Schiller G, Henne R, Borck V. Vacuum plasma spraying of high-performance electrodes for alkaline water electrolysis. J Therm Spray Technol 1995;4(2):185–94. https://doi.org/10.1007/BF02646111.
[32] Bertuccioli L, Chan A, Hart D, Lehner F, Madden B, Standen E. Study on development of water electrolysis in the EU. 2014.
[33] Zheng Y, Jiao Y, Qiao S, Vasileff A. Hydrogen evolution reaction in alkaline solution: from theory, single crystal models, to practical electrocatalysts. Angew Chem Int Ed 2017:7568–79. https://doi.org/10.1002/anie.201710556.
[34] Xie Y, Huang X, Wang J, Shao L, Willinger M, Yao Y. Ni/NiO nanoparticles on a phosphorous oxide/graphene hybrid for efficient electrocatalytic water splitting. J Mater Chem A 2017;5(28):14758–62. https://doi.org/10.1039/c7ta03628k.
[35] Wang H, Lee HW, Deng Y, Lu Z, Hsu PC, Liu Y, Lin D, Cui Y. Bifunctional non-noble metal oxide nanoparticle electrocatalysts through lithium-induced conversion for overall water splitting. Nat Commun 2015;6:1–8. https://doi.org/10.1038/ncomms8261.
[36] Lu Z, Xu W, Zhu W, Yang Q, Lei X, Liu J, Li Y, Sun X, Duan X. Three-dimensional NiFe layered double hydroxide film for high-efficiency oxygen evolution reaction. Chem Commun 2014;50(49):6479–82. https://doi.org/10.1039/c4cc01625d.
[37] Hnát J, Plevová M, Žitka J, Paidar M, Bouzek K. Anion-selective materials with 1,4-diazabicyclo[2.2.2]Octane functional groups for advanced alkaline water electrolysis. Electrochim Acta 2017;248:547–55. https://doi.org/10.1016/j.electacta.2017.07.165.
[38] Schalenbach M, Kasian O, Mayrhofer KJJ. An alkaline water electrolyzer with nickel electrodes enables efficient high current density operation. Int J Hydrogen Energy 2018;1–7. https://doi.org/10.1016/j.ijhydene.2018.04.219.
[39] Ju W, Heinz MVF, Pusterla L, Hofer M, Fumey B, Castiglioni R, Pagani M, Battaglia C, Vogt UF. Lab-scale Alkaline water electrolyzer for bridging material fundamentals with

realistic operation. ACS Sustain Chem Eng 2018;6(4):4829–37. https://doi.org/10.1021/acssuschemeng.7b04173.
[40] Salvi P, Nelli P, Villa M, Kiros Y, Zangari G, Bruni G, Marini A, Milanese C. Hydrogen evolution reaction in PTFE bonded raney-Ni electrodes. Int J Hydrogen Energy 2011;36(13):7816–21. https://doi.org/10.1016/j.ijhydene.2011.01.173.
[41] Kim JH, Lee JN, Yoo CY, Lee KB, Lee WM. Low-cost and energy-efficient asymmetric nickel electrode for alkaline water electrolysis. Int J Hydrogen Energy 2015;40(34):10720–5. https://doi.org/10.1016/j.ijhydene.2015.07.025.
[42] Trinke P, Haug P, Brauns J, Bensmann B, Hanke-Rauschenbach R, Turek T. Hydrogen crossover in PEM and alkaline water electrolysis: mechanisms, direct comparison and mitigation strategies. J Electrochem Soc 2018;165(7):F502–13. https://doi.org/10.1149/2.0541807jes.
[43] Borgardt E, Giesenberg L, Reska M, Müller M, Wippermann K, Langemann M, Lehnert W, Stolten D. Impact of clamping pressure and stress relaxation on the performance of different polymer electrolyte membrane water electrolysis cell designs. Int J Hydrogen Energy 2019;44(42):23556–67. https://doi.org/10.1016/j.ijhydene.2019.07.075.
[44] Ehelebe K, Seeberger D, Paul MTY, Thiele S, Mayrhofer KJJ, Cherevko S. Evaluating electrocatalysts at relevant currents in a half-cell : the impact of Pt loading on oxygen reduction reaction. J Electrochem Soc 2019;166(15):24–6. https://doi.org/10.1149/2.0911915jes.
[45] Bender G, Carmo M, Smolinka T, Gago A, Danilovic N, Mueller M, Ganci F, Fallisch A, Lettenmeier P, Friedrich KA, Ayers K, Pivovar B, Mergel J, Stolten D. Initial approaches in benchmarking and round robin testing for proton exchange membrane water electrolyzers. Int J Hydrogen Energy 2019;44(18):9174–87. https://doi.org/10.1016/j.ijhydene.2019.02.074.
[46] Miousse D, Lasia A, Borck V. Hydrogen evolution reaction on Ni-Al-Mo and Ni-Al electrodes prepared by low pressure plasma spraying. J Appl Electrochem 1995;25(6):592–602. https://doi.org/10.1007/BF00573217.
[47] Chang Liu, Carmo Marcelo, Guido Bender, Everwand Andreas, Lickert Thomas, Young James L, Tom Smolinka, Detlef Stolten WL. Performance enhancement of PEM electrolyzers through iridium-coated titanium porous transport layers. Electrochem commun 2018;97(October):96–9. https://doi.org/10.1016/j.elecom.2018.10.021.
[48] Vogt H, Balzer RJ. The bubble coverage of gas-evolving electrodes in stagnant electrolytes. Electrochim Acta 2005;50(10):2073–9. https://doi.org/10.1016/j.electacta.2004.09.025.
[49] Vogt H. The actual current density of gas-evolving electrodes - notes on the bubble coverage. Electrochim Acta 2012;78:183–7. https://doi.org/10.1016/j.electacta.2012.05.124.
[50] Janssen LJJ, Sillen CWMP, Barendrecht E, van Stralen SJD. Bubble behaviour during oxygen and hydrogen evolution at transparent electrodes in KOH solution. Electrochim Acta 1984;29(5):633–42. https://doi.org/10.1016/0013-4686(84)87122-4.
[51] Zhang D, Zeng K. Evaluating the behavior of electrolytic gas bubbles and their effect on the cell voltage in alkaline water electrolysis. Ind Eng Chem Res 2012;51:13825–32. https://doi.org/10.1021/ie301029e.
[52] Phillips R, Edwards A, Rome B, Jones DR, Dunnill CW. Minimising the ohmic resistance of an alkaline electrolysis cell through effective cell design. Int J Hydrogen Energy 2017;42(38):23986–94. https://doi.org/10.1016/j.ijhydene.2017.07.184.
[53] Chaudhari NK, Jin H, Kim B, Lee K. Nanostructured materials on 3D nickel foam as electrocatalysts for water splitting. Nanoscale 2017;9(34):12231–47. https://doi.org/10.1039/c7nr04187j.
[54] Li Y, Zhang H, Jiang M, Kuang Y, Sun X, Duan X. Ternary NiCoP nanosheet arrays: an excellent bifunctional catalyst for alkaline overall water splitting. Nano Res 2016;9(8):2251–9. https://doi.org/10.1007/s12274-016-1112-z.
[55] Zhu W, Yue X, Zhang W, Yu S, Zhang Y, Wang J, Wang J. Nickel sulfide microsphere film on Ni foam as an efficient bifunctional electrocatalyst for overall water splitting. Chem Commun 2016;52(7):1486–9. https://doi.org/10.1039/c5cc08064a.
[56] Tian J, Cheng N, Liu Q, Sun X, He Y, Asiri AM. Self-supported NiMo hollow nanorod array: an efficient 3D bifunctional catalytic electrode for overall water splitting. J Mater Chem A 2015;3(40):20056–9. https://doi.org/10.1039/c5ta04723d.
[57] Tang C, Cheng N, Pu Z, Xing W, Sun X. NiSe nanowire film supported on nickel foam: an efficient and stable 3D bifunctional electrode for full water splitting. Angew Chem Int Ed 2015;54(32):9351–5. https://doi.org/10.1002/anie.201503407.
[58] Rommal HEG. The role of absorbed hydrogen on the voltage-time behavior of nickel cathodes in hydrogen evolution. J Electrochem Soc 1988;135(2):343. https://doi.org/10.1149/1.2095612.
[59] Machado SAS, Tiengo J, de Lima Neto P, Avaca LA. The influence of H-absorption on the cathodic response of high area nickel electrodes in alkaline solutions. Electrochim Acta 1994;39(11–12):1757–61. https://doi.org/10.1016/0013-4686(94)85161-1.
[60] Soares DM, Kleinke MU, Torriani I, Teschke O. Deactivation mechanism of nickel cathodes in alkaline media. Int J Hydrogen Energy 1994;19(7):573–8. https://doi.org/10.1016/0360-3199(94)90214-3.
[61] Rommal HEG. Time-dependent energy efficiency losses at nickel cathodes in alkaline water electrolysis systems. J Electrochem Soc 1985;132(2):325. https://doi.org/10.1149/1.2113831.
[62] Hall DS, Bock C, MacDougall BR. The electrochemistry of metallic nickel: oxides, hydroxides, hydrides and alkaline hydrogen evolution. J Electrochem Soc 2013;160(3):F235–43. https://doi.org/10.1149/2.026303jes.
[63] Atkinson A, Taylor RI, Hughes AE. Oxidation by grain boundary diffusion - a quantitative demonstration of the mechanism. Int Corros Conf Ser 1983:110–4. No. August 2013.